Dielectric Properties and Optical Phonons in $LiNbO_3$

A. S. BARKER, JR., AND R. LOUDON*
Bell Telephone Laboratories, Murray Hill, New Jersey
(Received 8 December 1966)

The optical phonons and dielectric properties of $LiNbO_3$ have been studied by measurements of the infrared reflection spectra in the range 70 to 10 000 cm^{-1} and of Raman spectra for shifts in the range 10 to 900 cm^{-1}. Transmission measurements have also been made in the range 1000 to 10 000 cm^{-1}. The infrared data have been analyzed by oscillator fits to the reflectivity. These lead to values for the frequency, linewidth, and strength of each optical phonon. The optical-phonon frequencies are confirmed by the Raman measurements, which also give information on the variation of phonon frequency with direction of propagation. All except two of the infrared and Raman phonons predicted by group theory have been identified. The index of refraction in the transparent region from 900 to 24 000 cm^{-1} has been fitted analytically within the limits of experimental accuracy, by assuming the presence of a single ultraviolet oscillator in addition to the infrared phonon oscillators whose frequencies and strengths have been determined. The nature of the ferroelectric transition has been studied by means of group theory and by an investigation of lattice phonon-mode instabilities and Lorentz factors. The latter suggest that the transition in $LiNbO_3$ is similar to the transitions in the ferroelectric perovskites. In $LiNbO_3$, a lattice-vibration mode has been identified having the correct symmetry to cause the ferroelectric transition. This mode has a significant temperature dependence and a large Lorentz factor, favoring instability.

I. INTRODUCTION

THE compound $LiNbO_3$ is a crystalline insulator which is ferroelectric at room temperature.[1] Its optical properties in the visible and near infrared have attracted considerable attention recently, because of its large nonlinear polarization coefficients and the large negative birefringence which allows phase matching in optical-wave parametric-amplifier experiments.[2,3] $LiNbO_3$ is transparent from about 0.4 to 5.0μ wavelength.[1] Phonon combination bands limit the transparency at the long-wavelength end of this window and the infrared active phonons contribute to the index of refraction in the window region.

The primitive cell of $LiNbO_3$ contains two formula units which allow 27 degrees of freedom to be assigned to optical-phonon modes. According to Cochran's theory of ferroelectricity, some of these modes may be connected with the ferroelectric transition.[4] The present study was made to discover experimentally the infrared and Raman phonons in $LiNbO_3$ and to measure their strengths, frequencies, and linewidths. A search was made for possible transparent regions beyond the near infrared window but only two rather lossy windows were found. In addition, the group theory for the long-wavelength optical-phonon modes in the $LiNbO_3$ structure was correlated with the optical-mode study to find if any light could be shed on the nature of the ferroelectric transition ($T_c = 1190°C$[1]).

While this report was being written reports were received of infrared spectra of $LiNbO_3$ by Axe and O'Kane[5] (AK) and Raman spectra by Schaufele and Weber[6] (SW). There is much similarity between all the sets of data, though there are some significant differences and the interpretation presented here goes considerably beyond that given by AK and SW. The present authors have benefited from reading the preprints and reference will be made to them where appropriate below.

II. GROUP CHARACTER ANALYSIS

1. The Phase Transition

The structure of $LiNbO_3$ below the ferroelectric Curie point is well established.[7,8] The crystal space group is $R3c(C_{3v}^6)$ and the primitive cell contains two formula units. The rotations and reflections of the space group are listed together with the character table in Table I. The threefold rotation axis is parallel to the crystal c axis and the primitive cell can be chosen so that this axis passes through one of the Nb ions. The reflection planes σ_v contain the threefold axis and involve a nonprimitive translation τ, which connects the two Nb ions in the primitive cell.

In order to determine the probable crystal symmetry above the transition temperature, Abrahams *et al.*[9] have studied x-ray diffraction from $LiNbO_3$ in the temperature range 24 to 1200°C. They conclude that at the Curie temperature ($T_c = 1190°C$) the Nb ions become centers of inversion, and the Li ions become coplanar with triangles of O ions. Abrahams *et al.* suggest the space groups $R\bar{3}(C_{3i}^2)$ and $R\bar{3}c(D_{3d}^6)$ as candidates for the crystal symmetry group above the

* Present address: Physics Department, University of Essex, Colchester, England.

[1] K. Nassau, H. J. Levinstein, and G. M. Loiacono, J. Phys. Chem. Solids **27**, 983 and 989 (1966).

[2] G. D. Boyd, R. C. Miller, K. Nassau, W. L. Bond, and A. Savage, Appl. Phys. Letters **5**, 234 (1964).

[3] J. A. Giordmaine and R. C. Miller, Phys. Rev. Letters **14**, 973 (1965).

[4] W. Cochran, Advan. Phys. **9**, 387 (1960).

[5] J. D. Axe and D. F. O'Kane, Appl. Phys. Letters **9**, 58 (1966).

[6] R. F. Schaufele and M. J. Weber, Phys. Rev. **152**, 705 (1966).

[7] S. C. Abrahams, J. M. Reddy, and J. L. Bernstein, J. Phys. Chem. Solids **27**, 997 (1966).

[8] S. C. Abrahams, W. C. Hamilton, and J. M. Reddy, J. Phys. Chem. Solids **27**, 1013 (1966).

[9] S. C. Abrahams, H. J. Levinstein, and J. M. Reddy, J. Phys. Chem. Solids **27**, 1019 (1966).

TABLE I. Character table, vibrational modes, and selection rules for $LiNbO_3$ below the Curie point.

Space group $C_{3v}^6 = R3c$		Group operations $(E \mid 0)$	$2(C_3 \mid 0)$	$3(\sigma_v \mid \tau)$	Modes at $k=0$ Acoustic	Optic	Selection rules
Irreducible representations of C_{3v}.	A_1	1	1	1	1	4	IR$(E \mid \mid c)$, R
	A_2	1	1	−1		5	
	E	2	−1	0	1	9	IR$(E \perp c)$, R
Representations of general displacements of the atoms.	2Li	6	0	0	Selection rules		
	2Nb	6	0	0	R= Allowed Raman transition		
	6O	18	0	0	IR= Allowed infrared transition		

transition.[9,10] Observation of linear and nonlinear optical properties above T_c are consistent with both these space groups.[11]

The first of these possibilities can be ruled out by arguments based on the theory of phase transitions. According to the general theory of Landau,[12] a phase transition from a disordered to an ordered state is accompanied by the appearance of an order parameter and a reduction in the symmetry of the system. The expectation value of the order parameter is zero in the disordered phase (here $T > T_c$), but becomes different from zero in the ordered phase. For the case of $LiNbO_3$ the order parameter can be taken as the mean displacement of the Nb ions from their centers of inversion. In the disordered phase the crystal symmetry is characterized by a space group G. In the ordered phase the crystal structure is invariant only under those operations of G which leave the order parameter invariant. Except for a few special cases, this requirement results in the space group of the ordered phase being a subgroup of the space group of the disordered phase.

The space groups $R\bar{3}$ and $R3c$ contain the same number of rotation and reflection operations. If $R\bar{3}$ were the correct symmetry group above T_c, then on cooling the crystal through T_c the threefold rotation axis would be unchanged but the center of inversion symmetry would *disappear* and the reflection planes σ_v would *appear*. This behavior is inconsistent with the symmetry arguments outlined above. However $R\bar{3}c$ is acceptable for the space group above the transition temperatures. The ferroelectric space group $R3c$ is a subgroup of $R\bar{3}c$ and this pair of groups therefore satisfies the phase-transition symmetry requirements. The operations of $R\bar{3}c$ are listed along with the character table in Table II. An Nb ion is again taken as the origin for the rotation and reflection operations. The compatibility between the irreducible representations of the symmetry groups above and below the Curie temperature is given in Table III.

The displacement of the Nb and Li ions away from their equilibrium positions above T_c which takes the crystal into its ferroelectric structure below T_c is a distortion of A_{2u} symmetry in $R\bar{3}c$. The magnitude of this distortion is the order parameter for the phase transition. Below T_c Table III shows that A_{2u} becomes the scalar representation A_1 of the space group $R3c$. Thus the order parameter is correctly left invariant by the operations of $R3c$. Since the direct product

TABLE II. Character table, vibrational modes, and selection rules for $LiNbO_3$ above the Curie point.

Space group $D_{3d}^6 = R\bar{3}c$		$(E \mid 0)$	$2(C_3 \mid 0)$	$3(C_2 \mid \tau)$	$(I \mid 0)$	$2(S_6 \mid 0)$	$3(\sigma_v \mid \tau)$	Modes at $k=0$ Acoustic	Optic	Selection rules
Irreducible representations of D_{3d}	A_{1g}	1	1	1	1	1	1		1	R
	A_{2g}	1	1	−1	1	1	−1		3	
	Eg	2	−1	0	2	−1	0		4	R
	A_{1u}	1	1	1	−1	−1	−1		2	
	A_{2u}	1	1	−1	−1	−1	1	1	3	IR$(E \mid \mid c)$
	E_u	2	−1	0	−2	1	0	1	5	IR$(E \perp c)$
Representations of general displacements of the atoms	2Li	6	0	−2	0	0	0	Selection rules		
	2 Nb	6	0	0	−6	0	0	R= allowed Raman transition		
	6 O	18	0	−2	0	0	0	IR= allowed infrared transition		

[10] See footnotes in Ref. 9.
[11] R. C. Miller and A. Savage, Appl. Phys. Letters 9, 169 (1966).
[12] L. D. Landau and E. M. Lifshitz, *Statistical Physics* (Addison-Wesley Publishing Company, Reading, Massachusetts, 1958).

$A_{2u}\times A_{2u}\times A_{2u}=A_{2u}$ in the group $R\bar{3}c$, Landau's theory[12] shows that the phase transition can be either first or second order as far as the symmetry restrictions are concerned. Recent measurements suggest that it is second-order.[10,11] More detailed discussions of the application of Landau's theory to ferroelectric phase transitions can be found in Refs. 13–15.

2. Phonon Modes Above and Below T_c

The characters of the reducible representations generated by general displacements of the different types of ion in the unit cell are listed in the bottom rows of Tables I and II. The reduction of these representations has been carried out with the results shown in the right-hand columns of these tables. The selection rules for participation of the corresponding $\mathbf{k}=0$ vibrational modes in infrared absorption and Raman scattering are also shown.

Above the Curie point we find three infrared-active modes for the electric vector E parallel to the c axis and five for E perpendicular to the c axis. Below the Curie point the reduction in symmetry causes one additional mode to become active for E parallel to the c axis and four additional modes for E perpendicular to the c axis. The strength of the absorption due to these additional modes depends upon the magnitude of the order parameter. The experimental results show that some of the modes are only weakly absorbing and cannot be detected. This may be due to the dependence of their intensity on the order parameter. The group-character analysis was carried out above T_c in order to examine this effect; all the experimental results were taken in the ferroelectric phase below T_c. The number of Raman-active modes is five above T_c and thirteen below T_c.

TABLE III. Compatibility between representation above and below the Curie point.

D_{3d} representations	A_{1g}	A_{2g}	E_g	A_{1u}	A_{2u}	E_u
C_{3v} representations	A_1	A_2	E	A_2	A_1	E

The A_{2u}-symmetry vibration which corresponds to the ferroelectric distortion has a frequency which is predicted by the Cochran theory of ferroelectricity[4] to tend towards zero as the Curie temperature is approached from above.

The results in Table I for the vibrational symmetries below T_c are in agreement with the calculations of AK.[5]

III. EXPERIMENTAL METHODS

Single-crystal samples of $LiNbO_3$ about 1cm×1 cm×0.1 cm were used for the present study. The crystals were grown by K. Nassau of this laboratory using a specially developed technique which yields single-domain crystals of good optical quality.[1] After x-ray alignment, flat faces were polished using in succession water slurrys of Buehler 303½, then 305, then Linde C grinding compounds. Infrared reflection spectra were taken at room temperature for the electric vector E parallel to the c axis ($E \parallel c$ axis) and for $E\perp c$ axis. The methods used have been described previously.[16,17] These spectra are shown in Figs. 1 and 2. Transmission measurements were also made in the 1 to 10-μ region at room temperature. The reflection and transmission were reduced to yield ϵ'', the imaginary part of the dielectric constant. ϵ'' for each polarization is shown in the lower part of Figs. 1 and 2.

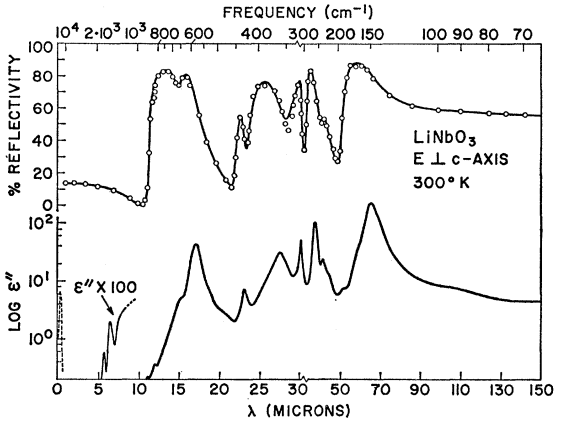

FIG. 1. Reflectivity and imaginary dielectric constant, ϵ'', of $LiNbO_3$ for $E\perp c$ axis. The solid curve through the experimental points is the best oscillator fit to the reflectivity and predicts the modes listed in Table IV. The imaginary part of ϵ shown for $\lambda>10$ μ results from a Kramers-Kronig transform of the experimental reflectivity. From 5 to 10 μ, ϵ'' is deduced from transmission measurements, and the peak near 0.24 μ results from fits to the index of refraction.

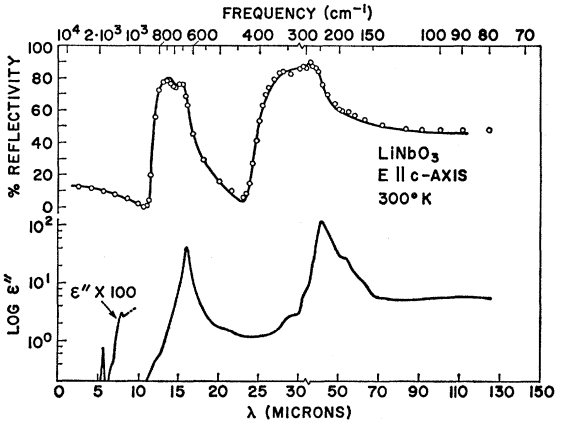

FIG. 2. Reflectivity and imaginary dielectric constant, ϵ'', of $LiNbO_3$ for $E \parallel c$ axis. The solid curve through the experimental points is the best oscillator fit to the reflectivity and predicts the modes listed in Table IV. Other details are the same as Fig. 1, except that the mode near 0.22 μ determined by the index fits is not shown since it has not been confirmed by uv spectroscopy.

[13] P. W. Anderson and E. I. Blount, Phys. Rev. Letters **14,** 217 (1965).
[14] C. Haas, Phys. Rev. **140,** A863 (1965).
[15] E. Ascher, Phys. Letters **20,** 352 (1966).
[16] A. S. Barker, Jr., Phys. Rev. **132,** 1474 (1963).
[17] W. G. Spitzer and D. A. Kleinman, Phys. Rev. **121,** 1324 (1961).

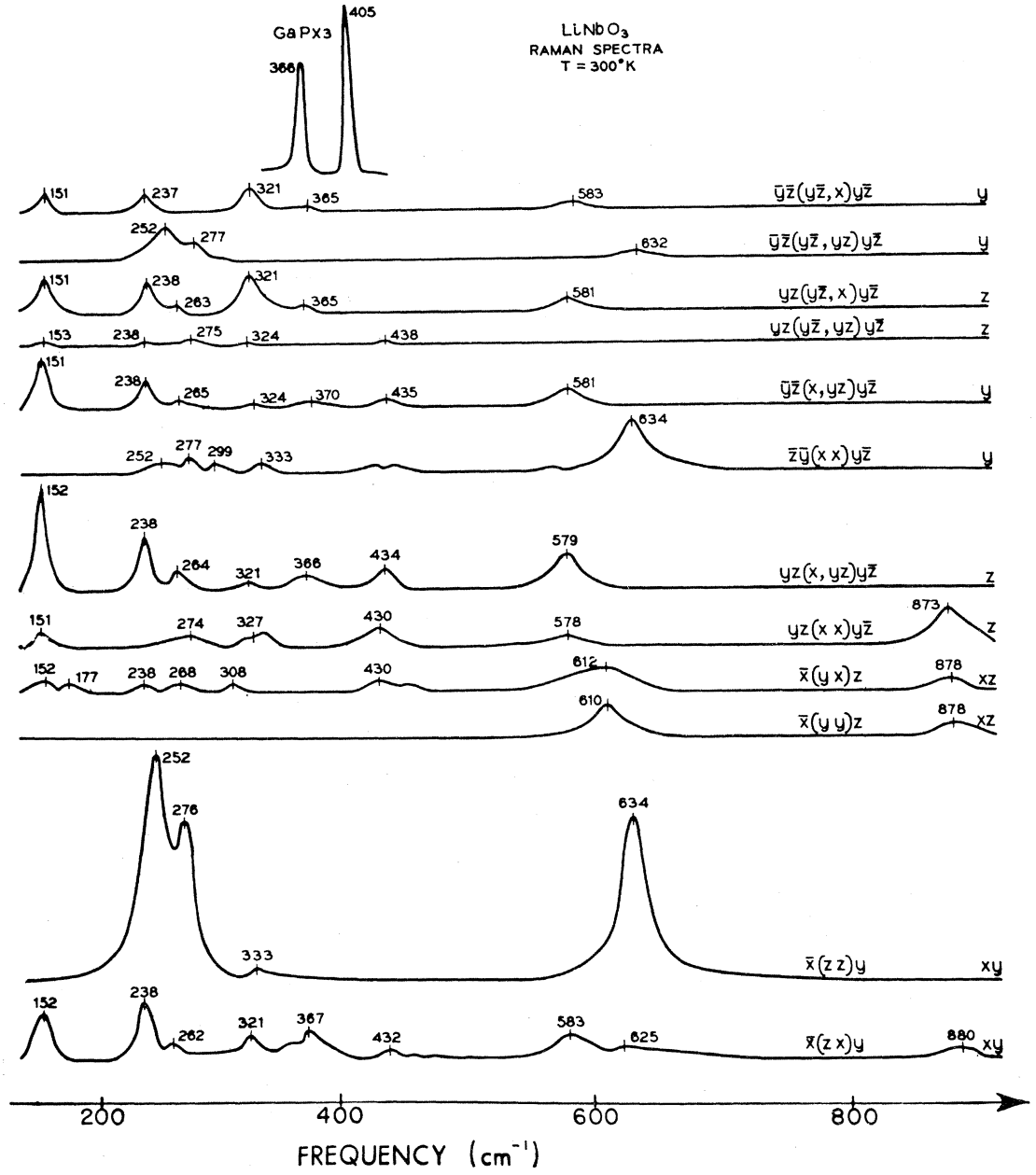

FIG. 3. Raman spectra of $LiNbO_3$. The symbols denoting polarization and scattering directions are explained in the text. The symbol at the far right gives the wave-vector direction of the scattered phonon. The spectra are all normalized as closely as possible to the same incident laser power and solid angle *in* the sample.

Raman spectra for 90° scattering angle were taken using a He-Ne 6328 Å laser. The general techniques and apparatus used were similar to those described by others.[18] Several configurations of incident and scattered beam direction and polarization relative to the crystal axes were used. Some of these spectra are shown in Fig. 3 for samples at 300°K. In addition, some spectra were taken with samples at temperatures between 300° and 525°K to check for mode frequency shifts. All Raman spectra were scanned down to a Raman shift of 10 cm^{-1}. No structure was found in the frequency range between 10 cm^{-1} and the 152-cm^{-1} lowest-frequency phonon. By using a 10^8 optical attenuator (several Kodak gelatin filters) absolute Raman scattering efficiencies were measured. This entailed taking a Raman spectrum then scanning the laser beam with the attenuator in place. The Raman spectrum of a crystal of GaP was also measured in order to compare

[18] T. C. Damen, S. P. S. Porto, and B. Tell, Phys. Rev. **142**, 570 (1966).

scattering efficiencies. This spectrum is shown scaled up by a factor of 2.5 in Fig. 3.

IV. EXPERIMENTAL RESULTS

1. Phonon Modes at 300°K

Figure 1 shows the phonon-mode structure observed in the infrared study. A Kramers-Kronig transform[16,17] of the reflectivity was made to obtain the dielectric constant $\epsilon=\epsilon'-i\epsilon''$. The Kramers-Kronig values for ϵ'' become very uncertain for wavelengths shorter than 10μ. In this region, we have used the values of ϵ'' obtained from the transmission experiments. In the spectrum of ϵ'' ($E\perp c$) there are eight transverse and eight longitudinal modes with strengths typical of infrared active phonons, though one of the weaker modes (15.3μ) may be a combination band. The very weak modes at 5.7, 6.5, and 12μ we assume to be two phonon combination bands. The band at 5.7 μ provides the attenuation which limits the transparency window extending from the visible into the near infrared and is twice the frequency of the highest fundamental longitudinal optic mode. Three-phonon absorption is very weak in this material since it would extend up to 3.8μ, but has not been observed in samples 1-cm thick. Figure 2 clearly shows at least two transverse and longitudinal modes for $E \parallel c$ axis with some additional weaker structure.

Oscillator fits to the reflectivity spectra were carried out to characterize the modes. Such fits allow more precise determination of the transverse and longitudinal mode frequencies than merely taking the high- and low-frequency inflection points in each reststrahlen band. In addition, the integrated strength of each mode is obtained directly without depending on the detailed shape of ϵ'' obtained from the Kramers-Kronig analysis. For the oscillator fits we take the dielectric function at frequency ν to be given by

$$\epsilon=\epsilon_\infty+\sum_j \frac{S_j\nu_j^2}{\nu_j^2-\nu^2+i\nu\gamma_j}, \qquad (1)$$

where S_j, ν_j, γ_j are the strength, frequency, and linewidth of the jth infrared active mode and ϵ_∞ is the frequency-independent part arising from the vacuum and high-frequency electronic processes. Discussions have been given previously of the relation of the transverse and longitudinal phonon frequencies to the oscillator parameters.[19] To a good approximation, we may take the oscillator-fit parameters ν_j as the transverse phonon frequencies. The group theory predicts that at room temperature for $E\perp c$ axis the sum must run over $j=1$ to 9 and for $E \parallel c$ axis $j=1$ to 4 (see Table I). In fact, we find fewer modes for $E\perp c$ axis as is discussed below.

The upper part of Table IV shows the mode parameters for the electric vector E perpendicular to the c axis. In addition to the transverse-mode parameters, we have listed the longitudinal-mode frequencies and linewidths. These latter are obtained from the complex zeros of the dielectric function[19] given by Eq. (1). A more complete discussion of the linewidths is given below.

The modes with $E \parallel c$ axis are listed in the lower part of the table. We find four transverse modes as predicted by group theory plus an additional mode at 692 cm^{-1}. Since the 692-cm^{-1} mode is not confirmed by the Raman spectra, we take it to be a second-order phonon combination band. The mode seen at 306 cm^{-1} in the infrared is somewhat puzzling, since that mode which we take to be the corresponding Raman mode is at 333 cm^{-1}. This discrepancy (26 cm^{-1}) is outside of experimental uncertainty and larger than the discrepancy in any other case where Raman and infrared data have been taken on the same modes. Johnston and Kaminow[20] have studied the 333-cm^{-1} Raman mode in detail, particularly by reducing the angular spread of the Raman beam to eliminate the possibility of any off-axis phonon modes with different scattering tensor being detected. They find that the 333 cm^{-1} mode maintains the same intensity relative to the other Raman phonons and also has the correct Stokes to antistokes intensity ratio for a fundamental. The infrared reflectivity shows an additional weak mode at 348 cm^{-1} with parameters $S=0.03$ and $\gamma=0.05$. The 307 mode (also reported by AK[5] at 305 cm^{-1}) is the stronger but the 344 cm^{-1} infrared mode is closer to the observed Raman frequency.

For $E\perp c$ axis we find seven fundamental infrared modes (confirmed by Raman peaks) and an additional mode at 670 cm^{-1} which we regard as a combination band since there is no confirming Raman peak and the $E \parallel c$ axis spectrum has a similar band at 692 cm^{-1} which we have assigned as a combination band. Since we are short two fundamental infrared phonons (Table I) it is tempting to call the 670-cm^{-1} mode a fundamental leaving only one missing fundamental. AK find that this mode becomes stronger when the surface of the crystal is etched. This behavior probably rules out the possibility of the 670 mode being a fundamental A_2 optic mode made infrared active by strains.[16] If the 670 mode is a two-phonon combination mode, any reasonable choice of the two fundamental components predicts that the mode should decrease in strength about 30% on cooling to 100°K. This experiment was done; however, the results remain ambiguous since the strong mode at 586 cm^{-1} (see Fig. 1) changes its strength, frequency, and damping enough to make analysis of the 670-mode strength very uncertain. Thus, there is at present no way of proving our assignment of the 670 mode as a combination band.

The reflectivity fits resulting from the oscillator parameters shown in Table IV are shown as solid

[19] A. S. Barker, Jr., Phys. Rev. **145**, 391 (1966).

[20] W. D. Johnston, Jr. and I. P. Kaminow (private communication).

TABLE IV. Optical phonon modes in $LiNbO_3$ at 300°K.

	$E \perp c$ axis Infrared			E-symmetry modes Raman		Mixed phonons with wave vector 45° from z axis	
				Pure	Phonons		
$\bar{\nu}_j(\text{cm}^{-1})$	S_j	$\gamma_j(\text{cm}^{-1})$	Polarization	$\bar{\nu}$	γ	$\bar{\nu}$	γ
152	22.0	14	t	152	17	177	13
198		(7)	l				
236	0.8	12	t	238	10		
238		(6)	l				
265	5.5	12	t	264	13		
296		(6)	l	299	12		
322	2.2	11	t	321	15		
342		(11)	l	333	15	308	~10
363	2.3	33	t	367	20	353	~20
418		(10)	l				
431	0.18	12	t	434	17	447	~20
450		(10)	l				
586	3.3	35	t	579	29	610	25
660[a]		(23)	l				
670[a]	0.2	47	t				
878		(15)	l	880	38	878	35
		$\epsilon_\infty = 5.0$		$\epsilon_\infty + \sum_j S_j = 41.5$			
	$E \parallel c$ axis			A_1 symmetry modes			
248	16.0	21	t	252	28		
273		(7)	l				
274	1.0	14	t	276	~20		
306		(12)	l				
307	0.16	25	t	333	13		
423		(12)	l				
628	2.55	34	t	634	28		
686[a]		(24)	l				
692[a]	0.13	49	t				
869		(17)	l	873	35		
		$\epsilon_\infty = 4.6$		$\epsilon_\infty + \sum_j S_j = 26.0$			

[a] Probably combination bands.

curves in the upper parts of Figs. 1 and 2. The reflectivity fit is quite satisfactory and the parameters are typical of ionic crystals. The lowest-frequency modes are discussed further in Sec. 6 and all the modes are used to fit the variation of the index of refraction with frequency (Sec. 4).

For the Raman spectra we use the notation of Ref. 18 to specify the input and scattered photon directions and polarizations. For the spectrum $x(yx)z$ we mean the input photon has its wave vector along x and its E vector along y. The scattered photon has its E vector along x and its k vector along z. 45° directions are specified by a double symbol. For example, xy specifies the direction bisecting the x and y axes. x, y, and z are orthogonal crystalline axes with z chosen as the c or hexagonal axis. There is some freedom in the choice of x and y. By convention x is chosen perpendicular to a mirror plane. This choice simplifies the polarizability tensor, and is the choice used in the present work.

It is important to realize that from k conservation a fundamental mode in the $x(yx)z$ spectrum results from a phonon mode with wave vector at 45° between the x and z axes. In a uniaxial crystal the frequency of this phonon will not necessarily be one of the natural modes seen in the infrared spectrum. Table IV shows which phonons have been observed in the pure spectra—i.e., with phonons scattered along z or perpendicular to the z axis. In cases where a phonon is seen in several polarizations we list the frequency of the strongest line. Nearly all the Raman frequencies lie within 1% of the corresponding infrared phonon frequencies and in all cases well within the experimental uncertainties encountered in determining the frequencies. It is apparent that most of the longitudinal modes have very small cross sections as they have not been detected in the Raman spectra. The column at the far right of Table IV indicates phonons detected propagating at 45° to the z axis. Some of these modes are weak and apparently become undetectable in the present experiments as the phonon wave vector is rotated into the xy plane where the modes become longitudinal E type modes or transverse A modes.

Figure 4 shows dispersion curves constructed from the infrared and Raman data. We have not shown the region of very small k vector where polariton effects are important, because the present 90° scattering experiments measure phonons whose wave vectors ($k = 2\pi/\lambda \sim 3 \times 10^5$ cm^{-1}) are well outside the polariton

region. This connection scheme in Fig. 4 is tentative because the positions of the undetected modes are unknown, and "no-crossing" rules apply to the vibrational energies. The variation of phonon frequency with direction of **k** is clearly seen in the Raman spectra, particularly for the modes close to 177, 600, and 880 cm^{-1}. Such direction-dependent phonon frequencies have also been observed in recent work[18] on ZnO and in earlier experiments (see Ref. 22 for a review).

The results given in Table IV can be compared with those of AK[5] and SW.[6] For the infrared absorption measurements AK interpreted their data in terms of lattice modes by determining the positions of the maxima in ϵ'' obtained by Kramers-Kronig analysis. For $E \perp c$ they obtain eight transverse oscillation frequencies in fair agreement with our frequencies listed in the upper part of Table IV, the average discrepancy being about 10 cm^{-1} to the low side. The agreement in the oscillator strengths is less satisfactory. The oscillator fitting procedure used in the present paper may yield the more reliable strengths. For $E \parallel c$, AK obtained oscillators at 248, 305, and 605 cm^{-1} in rough agreement with ours, but they also have an oscillator at 187 cm^{-1}. We believe the 187-cm^{-1} mode arises from a spurious bump on the reflectivity curve of AK (Axe in private communication has agreed with this conclusion). AK's 305 mode agrees well with the mode we observe at 307. We have already discussed the anomalous shift of this mode frequency from the Raman mode at 333 cm^{-1}.

Our Raman frequencies agree well with those measured by SW[6] and we have observed all the lines reported by them. On the other hand, SW do not observe the longitudinal modes at 299 and 873 cm^{-1}.

The close agreement between our oscillator frequencies determined from the reflectivity, and those determined by Raman spectroscopy indicate that the oscillator fit to the reflectivity is a more accurate method of analysis than that employed by AK.

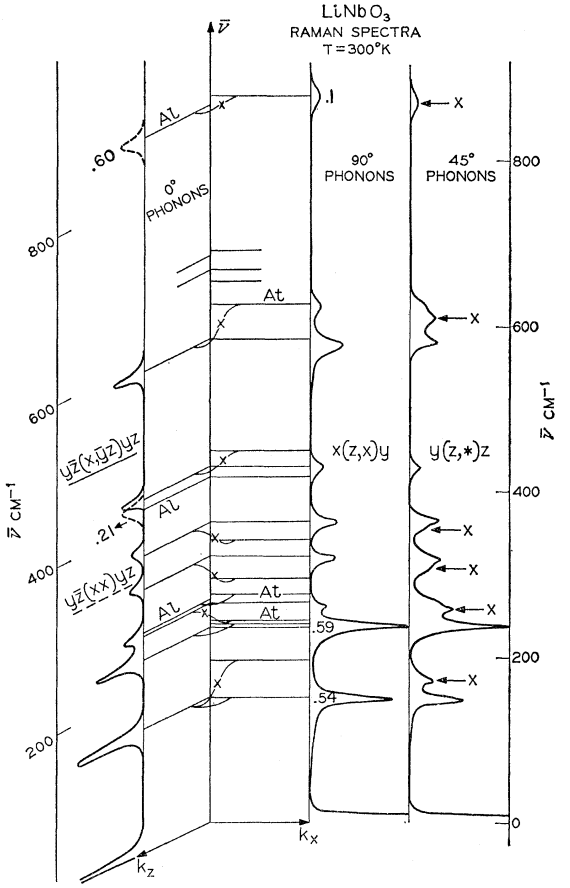

FIG. 4. Long-wavelength phonon-dispersion curves for $LiNbO_3$. Curved lines show the most likely bending of the phonon branches with θ, the angle between the phonon wave vector and the z axis. The crosses mark intermediate phonons which have been observed. The weak A_1 mode at 307 cm^{-1} is omitted for clarity. The weak modes shown near 700 cm^{-1} are probably combination bands, though they are strong enough to have split transverse and longitudinal components (Table IV). The Raman scattering strengths are listed near some modes; these must be multiplied by 10^{-6}/(cm sr) to give standard units (see text). * denotes unpolarized scattered light; x and y components were present.

2. Phonon Damping

The linewidths of the transverse infrared-active phonons are given in Table IV. The values are the γ_j values used in the reflectivity fits and are typical of modes in ionic materials. The oscillator representation of the dielectric function [Eq. (1)] with the constant damping parameters γ_j often fits the reflectivity spectra very well for all frequencies though it may describe the loss spectrum (ϵ'') rather poorly far from the transverse modes or poles (i.e., far from any ν_j). A test of the adequacy of Eq. (1) to describe ϵ'' accurately can be made by examining the longitudinal phonon linewidths. We first note that transverse phonons correspond to the poles of ϵ and the phonon widths correspond to the widths of the peaks in the spectrum of $\epsilon'' = \mathrm{Im}(\epsilon)$. Longitudinal phonons correspond to the poles of ϵ^{-1} and the longitudinal-phonon linewidths will correspond to the widths of the peaks of the spectrum of $\mathrm{Im}(\epsilon^{-1})$. We test the adequacy of Eq. (1) by listing the linewidths in the $\mathrm{Im}(\epsilon^{-1})$ spectrum in Table IV. These linewidths are all enclosed in brackets since we expect Eq. (1) to be only an approximation to the true ϵ of the crystals, especially for frequencies far from the transverse modes. We may compare the bracketed linewidths now with the directly measured Raman linewidths for those longitudinal phonons which could be detected. In making the comparison we must realize that the usual uncertainty in determining an infrared linewidth is $\pm 20\%$. Even so we see that the longitudinal linewidths in some cases (e.g., the highest frequency longitudinal modes) are in disagreement. The peak positions, however, in the $\mathrm{Im}(\epsilon^{-1})$ spectrum are in good agreement with the Raman-mode frequencies. Thus, we can get longitudinal-mode frequencies

from Eq. (1) but cannot expect accurate longitudinal-mode linewidths.

We note from Figs. 1 and 2 that combination-band phonons limit the transparency window in the near infrared. A search was made for additional windows in the far infrared spectral region. The Kramers-Kronig loss spectra show that except for two very lossy windows near 21μ (470 cm^{-1}) and 47μ (210 cm^{-1}) the attenuation coefficient α remains above 6000 cm^{-1} from the near infrared limit to frequencies below the lowest infrared-phonon mode. The "window" at 21 μ has $\alpha=2500$ cm^{-1} for $E \| c$ axis and $\alpha=3600$ cm^{-1} for $E \perp c$. At 47 μ, $\alpha=2400$ cm^{-1} for $E \perp c$. We use the convention that the electric field of a plane wave attenuates with distance travelled (x), as $E \sim \exp(-\alpha x/2)$. Since the window at 21 μ is controlled by the fundamental transverse-phonon modes, we can make some estimate of how this window may open with cooling. In the heating Raman experiment, we observe that the 628-cm^{-1} $E \| c$ phonon broadens as $T^{1.5}$. Approximating this phonon by our standard form [Eq. (1)], this temperature dependence should cause $\alpha(21\mu, E \| c)$ to drop from 2500 to 1200 on cooling to 150°K. Below 150°K the window may open further, however, we are in the "sum-band" region and cannot expect to get complete transparency even by going to $T=0$. The low-frequency window below all infrared modes may open much more dramatically. Estimates are difficult, however, since the loss in this region involves sum and difference phonon bands.

3. Raman Strengths

In addition to the Raman frequencies listed in Table IV, we have also determined the strengths of some of the more prominent Raman lines. These are indicated on Fig. 4 by the numbers having order of magnitude 10^{-6}. The strengths represent the fraction of the incident laser light which is scattered into the appropriate Raman line per cm path length in the crystal per unit steradian in the direction of observation indicated. They were determined by comparing the light intensities in the spectrometer of the Raman line itself and of the exciting laser light, which was reflected directly into the spectrometer by a mirror. The laser light was first attenuated by a factor of 10^8 using commercially available gelatin-filter attenuators. The acceptance angle of the spectrometer and the geometrical factors associated with the crystal mounting and the laser beam were carefully measured to provide the best possible values for the absolute intensities. Nevertheless, there remain uncertainties in the comparison of the laser and Raman intensities due to the different cross-sectional shapes of the two beams, and to the different properties of the phototube and grating at the slightly different frequencies of the two beams. We estimate Raman strengths to be accurate to within a factor of 2; the relative strengths are accurate to about $\pm 40\%$. We note that the integrated strength of the Raman spectrum is of order 10^{-6}, in agreement with a rough theoretical prediction of Raman strengths to be expected in crystals.[21]

The relative strengths of the Raman lines for varying polarizations and directions of propagation of the incident and scattered beams are in principle determined by the symmetry of the crystal. For general directions of photon and phonon propagation and polarization in $LiNbO_3$ the dependence of the strength R of a given Raman line on the polarization is given by[22]

$$R=[\epsilon_i^x\epsilon_s^x(c\xi^y+a\xi^z)+\epsilon_i^y\epsilon_s^y(-c\xi^y+a\xi^z)+\epsilon_i^z\epsilon_s^z b\xi^z + (\epsilon_i^y\epsilon_s^z+\epsilon_i^z\epsilon_s^y)d\xi^y+(\epsilon_i^z\epsilon_s^x+\epsilon_i^x\epsilon_s^z)d\xi^x + (\epsilon_i^x\epsilon_s^y+\epsilon_i^y\epsilon_s^x)c\xi^x]^2. \quad (2)$$

In this expression $\boldsymbol{\varepsilon}_i$ and $\boldsymbol{\varepsilon}_s$ are the polarization vectors of the incident and scattered light, ξ is the phonon polarization, and a, b, c, and d are coefficients which are characteristic of a given Raman line. The Cartesian axis z is parallel to the c axis, x is perpendicular to one of the three glide planes $(\sigma_v \mid \tau)$, and y is perpendicular to x and z. It is not difficult to verify that the expression for R is invariant under the 120° rotations C_3 about the z axis and under the glide plane operations $(\sigma_v \mid \tau)$.

All the selection rules for the Raman lines which can appear in the spectrum for any given scattering geometry are implicitly contained in Eq. (2). For example, comparing the fifth and sixth spectra in Fig. 3 the E transverse modes with $\mathbf{k}$ along y have polarization component ξ^z and thus with reference to Eq. (2) cannot contribute to the sixth spectrum where only the $\epsilon_i^x\epsilon_s^x$ term is nonvanishing. On the other hand, the A_1 transverse modes have polarization component ξ^z and thus cannot contribute to the fifth spectrum where only the $\epsilon_i^x\epsilon_s^y$ and $\epsilon_i^x\epsilon_s^z$ terms are nonvanishing. The variation of intensity of Raman scattering with the direction of propagation of a given mode is also in principle predictable from Eq. (2), though the calculation is very difficult in practice for a crystal as complex as $LiNbO_3$.

It is evident from Figs. 3 and 4 and Table IV that the scattering by purely transverse modes is more intense than the scattering by purely longitudinal modes. We have in fact been unable to detect many of the purely longitudinal modes. In following a given mode from a direction of $\mathbf{k}$ where it is purely transverse to a $\mathbf{k}$ direction where it is purely longitudinal the strength of the scattering is theoretically expected to vary because of the existence of the long-range electric fields associated with longitudinal polarization.[22] These same fields are the cause of the variation of mode frequency with θ. They lead to an additional scattering mechanism and produce a dependence of a, b, c, and d in Eq. (2) on the direction of $\mathbf{k}$. According to theory, the additional scattering due to the longitudinal com-

[21] R. Loudon, Proc. Roy. Soc. (London) **A275**, 218 (1963).
[22] R. Loudon, Advan. Phys. **13**, 423 (1964).

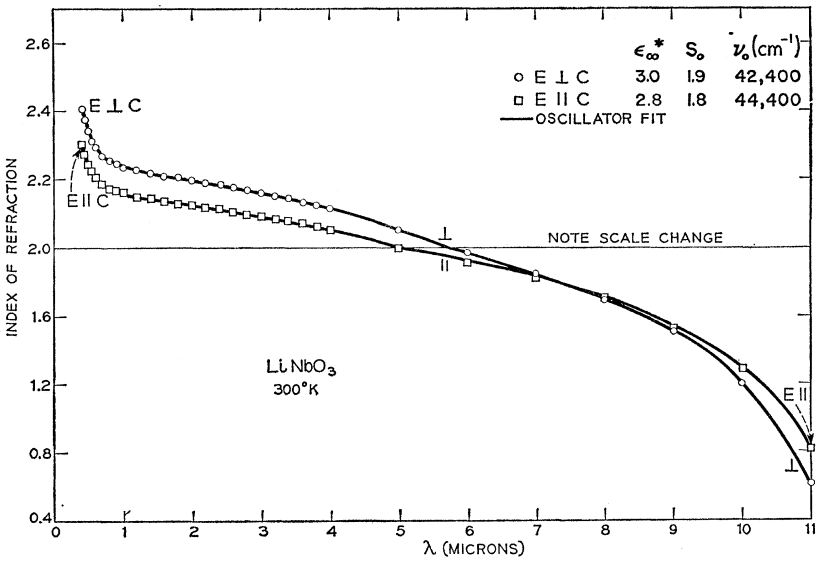

FIG. 5. Index of refraction of $LiNbO_3$. The data points for $\lambda<5$ μ were taken from Ref. 2. The solid curves are least-square fits using the ir phonon mode sand one adjustable oscillator in the uv. The best-fit uv-mode parameters are listed in the figure [see Eq. (4) for notation.]

ponent of a mode can interfere either destructively or constructively with the background scattering which is always present irrespective of the mode polarization. Evidently for $LiNbO_3$ a destructive interference occurs as the mode polarization is changed to longitudinal. This contrasts with the well-known case[23] of cubic ZnS where the longitudinal mode scattering is an order of magnitude more intense than the transverse mode scattering. The occurrence of constructive or destructive interference for longitudinal mode scattering depends on the relative signs of matrix elements which it is not feasible to calculate.

4. Index of Refraction in the Visible and Near Infrared

At wavelengths shorter than about 10 μ Figs. 1 and 2 show that ϵ'' is relatively small, i.e., less than 0.1. In this region the optical properties are determined mainly by the real part of the dielectric constant ϵ. The refractive indices of $LiNbO_3$ ($n=\sqrt{\epsilon}$) are of interest for the design of optical parametric amplifiers and other nonlinear devices where the achievement of phase-matching of the light waves is important. Figure 5 shows experimental values for n derived from our reflectivity measurements and from Ref. 2. For phase-matching work it is useful to have an analytic expression for the ordinary and extraordinary refractive indices as functions of frequency. We have fitted the refractive index n to expressions of the form

$$n=(\epsilon^*)^{1/2}, \tag{3}$$

where

$$\epsilon^*=\epsilon_\infty{}^*+[S_0\nu_0^2/(\nu_0^2-\nu^2)]+\sum_j[S_j\nu_j^2/(\nu_j^2-\nu^2)]. \tag{4}$$

In this expression S_0 and ν_0 are the strength and frequency of a single oscillator in the ultraviolet which is included to reproduce the sharp rise in n at the short wavelength end of Fig. 5 due to the onset of electronic transitions. Equation (4) has the standard Sellmeier form. The constant contribution $\epsilon_\infty{}^*$ includes the parts arising from the vacuum and from all the electronic processes having frequencies higher than ν_0. Finally, S_j and ν_j are the strengths and frequencies of the infrared transitions as in Eq. (1) and are listed in Table IV.

Equation (4) has been fitted to the experimental points in Fig. 5 by a least-squares computer calculation taking S_j and ν_j from Table IV and allowing $\epsilon_\infty{}^*$, S_0, and ν_0 to vary. The best least squares fits are shown by the solid lines in Fig. 5. The corresponding values of the parameters are listed in Fig. 5. For the frequency region of the reflectivity measurements of Figs. 1 and 2, $\nu\ll\nu_0$ and the first two terms in (4) are constant. Their combined value, $\epsilon_\infty{}^*+S_0$, should be closely equal to the constant term ϵ_∞ assumed in Eq. (1) in order to fit the infrared reflectivity, and this is confirmed.

The errors in the fits to the experimental points are of order $\Delta n\sim0.005$ at the long-wavelength end where the experimental data are also uncertain to the same extent. At the short-wavelength end, where the accuracy of the experimental data is much higher, the theoretical fit is correspondingly better, the typical discrepancy being about $\Delta n\sim0.0005$. In this connection, Miller[24] has pointed out that the birefringence important for second harmonic generation can vary by up to 0.004 from one sample to another. Boyd *et al.*[25] have also found that in parts of the visible region the ordinary index may vary by as much as 0.005 from one sample to another. It is apparent then, that for high precision, index measurements must be made on each sample for which the Sellmeier equation (4) is desired. For fits in the visible and out to 4 μ, the lattice-

[23] L. Couture-Mathieu and J. P. Mathieu, Compt. Rend. **236**, 371 (1953).

[24] R. C. Miller (private communication).

[25] G. D. Boyd, W. L. Bond, and H. L. Carter, J. Appl. Phys. **38**, 1941 (1966).

mode parameters we have given are probably suitable for any sample, since they enter the precision of the expression in this range in a relatively minor way.

Hobden and Warner[26] have fitted equations to the dielectric constant of $LiNbO_3$. They consider a narrower frequency range than that considered here but have included temperature dependence. Their results suggest that $\lambda_0=1/\nu_0$ and S_0 for both polarizations increase with temperature. Their values of $S_0+\epsilon_\infty{}^*$ are 0.2% higher and 1.0% lower for $E\perp$ and $E\parallel c$ axis, respectively. A more serious disagreement is in the values for λ_0, their values being 10% lower. It must be realized that because Eq. (4) is being fit in a region between resonances, a precision of 0.1% is easily obtainable in ϵ^* with parameters precise to only 1%; for example, a high value of $\epsilon_\infty{}^*$ can be compensated for by a low value of S_0. The 10% discrepancy in λ_0 values, however, seems outside the precision limits. For the case of $E\perp c$, it is possible to make an independent check of ν_0 of the ultraviolet oscillator since Kurtz, Rich, and Cole[27] have measured the uv reflectance spectrum of $LiNbO_3$. Their results show a peak in ϵ'' at 5.2 eV (0.238μ) in good agreement with $\lambda_0=0.236$ μ deduced from the least-squares fit.

5. Low-Frequency Dielectric Constants

The infrared measurements allow us to predict the dielectric constants at frequencies below all phonon modes (but above any piezoelectric resonances). From Table IV we note that the values for ϵ_0 are 41.5 for $E\perp c$ and 26.0 for $E\parallel c$. There is good agreement between our value of 26.0 and the value 27.7 given by AK.[5] For $E\perp c$ our value is 10% below the value given by AK, the two values happen to be about equally spaced above and below an independently measured value of 43 obtained in the microwave region.[28] A study of some initial oscillator fits to the data using incorrect mode strengths suggests that the accuracy of our values of ϵ_0 is about $\pm 5\%$.

As the frequency is decreased to very low values ($\sim$2 Mc/sec for a crystal 1-mm thick) the dielectric constant of $LiNbO_3$ goes through one or several resonances and increases from the clamped value $\epsilon_0{}^S$ to the free value $\epsilon_0{}^T$. Nassau *et al.*[1] have shown dispersion of this type from values in reasonable agreement with the infrared values given above to higher values at $\nu=10^5$ cps. This low-frequency dispersion is very strong for $E\perp c$, where ϵ_0 increases from 41.5 to about 77.0 (at 300°K). The strength of this dispersion is related to the electromechanical coupling constant k, by

$$k^2=(\epsilon_0{}^T-\epsilon_0{}^S)/\epsilon_0{}^T, \tag{5}$$

which yields the extremely large coupling constant of $k\sim 0.7$ for the $E\perp c$ geometry.

Thus, at very low frequencies about half of $\epsilon_0{}^T(E\perp c)$ and about 90% of $\epsilon_0{}^T(E\parallel c)$ comes from phonons. The temperature dependence of ϵ_0 appears to be almost entirely connected with the phonons. The spectrum of ϵ_0 just translates as a whole (even in the region of the electromechanical resonances) rising with increasing temperature.[1] The connection of the temperature dependence of ϵ with phonon frequency shifts is discussed below.

6. Phonon Instabilities

Cochran's theory of the ferroelectric transition applied to $LiNbO_3$ suggests that an A_{2u} phonon mode becomes unstable, i.e., has its frequency approach zero, at T_c.[4] The change of the mode frequency with temperature produces the temperature dependence of ϵ_0. As the temperature is reduced to T_c, other modes, for example the lowest E mode, can also approach instability by the same type of mechanism which reduces the restoring forces for the A_{2u} mode. The actual transition is accomplished of course by the mode which becomes unstable first. The lattice vibrations below T_c may also be unstable leading to a second transition as in $BaTiO_3$ or they may remain "soft," i.e., very temperature-dependent with a large strength and low frequency but not become unstable to the point of allowing a second phase transition. In $LiNbO_3$ there have been reports of additional transitions below T_c[29,30,10]; the smooth temperature dependence[1] of ϵ_0 suggests, however, that the phonon modes are somewhat soft, but that no transitions involving infrared phonons occurs in the temperature range where ϵ_0 has been measured.

We would expect that if the crystallographic change in structure at T_c is not too drastic the phonons seen below T_c are closely related to the unstable modes above T_c. We now examine the stability of the phonon modes for temperatures below T_c. Writing the Lyddane-Sachs-Teller relation[31] in differential form for a multimode crystal with zero damping, we have

$$\frac{d\epsilon_0}{\epsilon_0}=\frac{2d\nu_{l1}}{\nu_{l1}}+\frac{2d\nu_{l2}}{\nu_{l2}}+\cdots-\frac{2d\nu_{t1}}{\nu_{t1}}-\frac{2d\nu_{t2}}{\nu_{t2}}-\cdots, \tag{6}$$

where ν_{tj} are transverse phonon frequencies, and ν_{lj} are the longitudinal phonon frequencies. All quantities refer to the same polarization. We check $E\parallel c$ first and consider the temperature increment $\Delta T=100$°K. The low-frequency data[1] for ϵ_0 give $d\epsilon_0/\epsilon_0=0.058$ for the left side of Eq. (6). Figure 6 shows the mode shifts detected in the heating experiments. Using a linear fit to the shifts observed, for $\Delta T=100$°C the 625-cm^{-1} mode

[26] M. V. Hobden and J. Warner, Phys. Letters **22,** 243 (1966).
[27] S. K. Kurtz, T. C. Rich, and W. J. Cole, *Proceedings of the International Meeting on Ferroelectricity* (Institute of Physics, Czechoslovak Academy of Sciences, Prague, 1966).
[28] I. P. Kaminow and E. H. Turner, Proc. IEEE **54,** 1374 (1966).
[29] G. A. Smolenskii, N. N. Krainik, N. P. Khuchua, V. V. Khdanova, and I. E. Mylnikova, Phys. Status Solidi **13,** 309 (1966).
[30] See also Ref. 11 for arguments against extra phase transitions.
[31] A. S. Barker, Jr., Phys. Rev. **136,** A1290 (1964).

shifts -6.2 cm^{-1} and the 248-cm^{-1} mode shifts -4.2 cm^{-1}. These modes, then, contribute 0.020 and 0.034, respectively, to the right side of Eq. (6) and account for 93% of the observed value of $d\epsilon_0/\epsilon_0$. (Low-temperature infrared measurements of the longitudinal modes at 420 and 870 cm^{-1} show that they shift less than 1% on cooling $\Delta T=200$°C; these longitudinal modes then contribute much less than the transverse modes to $d\epsilon_0/\epsilon_0$.) The lowest A_1 transverse mode (248 cm^{-1}) is relatively the softest, contributing the largest part to the temperature dependence of ϵ_0. Though we have measured its temperature dependence only below T_c, it seems reasonable that this mode is closely related to an unstable A_{2u} Cochran-type mode which exists above T_c. We discuss possible ion motions for this mode below.

For $E\perp(c$ axis) using measured values of $\epsilon_0(T)$[1] and the same temperature increment $\Delta T=100$°C we have $\Delta\epsilon_0/\epsilon_0=0.031$. Figure 6 shows the shift of the soft 150 cm^{-1} E mode with temperature. From Fig. 6 we find $-2dv_t/v_t=0.022$ for $\Delta T=100$°C. This mode then makes the major contribution (70%) to the temperature dependence of ϵ_0 for this axis. The large strength, low frequency, and temperature dependence of this mode show that it also is somewhat unstable. The E_1 mode that corresponds to this mode above T_c must be more stable than the A_{2u} mode, however, since an E type mode does not cause the transition at T_c. We return now to a discussion of the soft A_1 mode at 248 cm^{-1}. It is instructive to note the $LiNbO_3$ is a distorted perovskite with the (111) axis of the perovskite corresponding to the c axis of $LiNbO_3$. Comparisons of $LiNbO_3$ with the perovskites must be made with care however, since the structures are far from being identical. For example, in the titanate perovskites the Ti ion is very loose in the surrounding oxygen cage. This fact led to the early "rattling Ti ion" theory of the ferroelectric transition. In the case of $LiNbO_3$, the ionic radii and the known structure parameters suggest a very close fit of Li and Nb ions in the oxygen framework. In the perovskites it is the Lorentz local field factor which favors phonon mode instabilities[32,33] and we investigate these below for $LiNbO_3$.

Cowley has fitted a shell model to the perovskite $SrTiO_3$ in its paraelectric phase at 90°K where the lowest-frequency mode is quite soft.[34] Table V shows the shell-model ion amplitudes and charges for the soft mode. We take the ion motions in the [001] direction. Cowley finds that all the positive ions move against all the negative ions in the soft mode, which fits our intuitive guess for the displacements of a mode which has so much dipole strength. We show the $SrTiO_3$ ion motions in Fig. 7. In addition, the main bond being

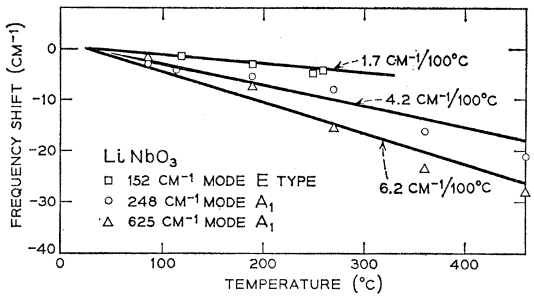

FIG. 6. Temperature dependence of phonon frequencies. The shifts were measured in the Raman spectra and are used to compare the stability of the modes shown.

compressed in the soft mode is the one linking Ti and O_1. This bond then makes up a large part of the restoring force. This is just the bond, however, which has the largest positive Lorentz factor, which lowers the restoring force, leading to a very low mode frequency. This feature of the lattice dynamics in the perovskites has been discussed in detail before.[34] The problem is only discussed qualitatively here as we will not fit a shell model to $LiNbO_3$. Table V lists the Lorentz local field factors for $SrTiO_3$ and $LiNbO_3$ between several ion pairs for long wavelength transverse vibrations ($\mathbf{k}\simeq 0$). We define the Lorentz factor as $\beta(l, l')$

$$\mathbf{E}_{loc}(l)=\mathbf{E}_0+\sum_{l'}\beta(l, l')\,\mathbf{P}(l'),$$

where $\mathbf{E}_{loc}(l)$ is the local field produced at ion l by the polarization $\mathbf{P}$ of ions of type l'. $\mathbf{E}_0$ is the applied macroscopic field. We take the phonon wave vector $\mathbf{k}$ to be along the x axis. For P along y or z we are dealing with transverse waves, but for P along x the wave is longitudinal and β_{xx} must include the depolarization field -4π. For $SrTiO_3$ (Table V) we list only β_{zz}, the full tensors are listed in Ref. 34. The large Lorentz factor discussed above for $SrTiO_3$ is $\beta(\mathrm{Ti}, O_1)=34.271$ (see Table V). There are two other features of the soft ferroelectric modes we should note. Not all Lorentz factors for this mode lower the frequency. For example, in $SrTiO_3$ $\beta(\mathrm{Ti}, O_2)$ raises the restoring force between these atoms. We observe however that in the soft mode these latter atoms undergo motion which involves bond *bending* rather than stretching. Cowley finds the restoring force for such bonds small and sometimes negative thus a large positive Lorentz factor is not needed here to cause instability. The second point is that when a material makes the ferroelectric transition, the low-frequency mode gets *frozen in* to provide the polar form of the crystal.[4,35]

Most of the Lorentz factors change very little on going through the transition. $\beta(\mathrm{Ti}, O_1)$ is 34.271 above T_c and actually increases to 34.316 below T_c for $SrTiO_3$ and $BaTiO_3$,[36] though the soft mode restoring force

[32] C. Kittel, *Introduction to Solid State Physics* (John Wiley & Sons, Inc., New York, 1956), 2nd ed., Chap. 8.
[33] A. S. Barker, Jr., *Symposium on Ferroelectricity* (Elsevier Publishing Company, Amsterdam, 1967).
[34] R. A. Cowley, Phys. Rev. **134**, A981 (1964).
[35] P. C. Kwok and P. B. Miller, Phys. Rev. **151**, 387 (1966).
[36] R. A. Cowley, Acta Cryst. **15**, 687 (1962).

TABLE V. Mode displacements and Lorentz factors in $SrTiO_3$ and $LiNbO_3$ above T_c.

Ion	Displacement (Å) along [001] in soft *TO* mode $SrTiO_3$	Charge (units of e)	Mass (amu)	Lorentz local-field factors β Sr versus ion at left	Ti versus ion at left
Sr	0.022	1.26	88	4.189	4.189
Ti	0.077	4.64	48	4.189	4.189
O_1	−0.093	−1.97	16	−4.479	34.271
O_2	−0.129	−1.97	16	8.523	−10.85
O_3	−0.129	−1.97	16	8.523	−10.85
		$LiNbO_3$		Li_1 versus ion at left	Nb_1 versus ion at left
Li_1	0.51	1	6.9	$\begin{pmatrix}-8.06 & 0 & 0\\ 0 & 4.50 & 0\\ 0 & 0 & 3.56\end{pmatrix}$	$\begin{pmatrix}-7.76 & 0 & 0\\ 0 & 4.80 & 0\\ 0 & 0 & 2.96\end{pmatrix}$
Li_2	0.51	1	6.9		
Nb_1	0.062	5	93	$\begin{pmatrix}-7.76 & 0 & 0\\ 0 & 4.80 & 0\\ 0 & 0 & 2.96\end{pmatrix}$	$\begin{pmatrix}-8.06 & 0 & 0\\ 0 & 4.50 & 0\\ 0 & 0 & 3.56\end{pmatrix}$
Nb_2	0.062	5	93		
O_1	−0.19	−2	16	$\begin{pmatrix}13.87 & 22.47 & 0.21\\ 22.47 & 0.50 & -0.36\\ 0.21 & -0.36 & -14.36\end{pmatrix}$	$\begin{pmatrix}-3.94 & -14.76 & 16.50\\ -14.76 & -0.55 & -11.91\\ 16.50 & -11.91 & 4.49\end{pmatrix}$
O_2	−0.19	−2	16		
O_3	−0.19	−2	16		
O_4	−0.19	−2	16		
O_5	−0.19	−2	16		
O_6	−0.19	−2	16	$\begin{pmatrix}-14.91 & -3.14 & -5.09\\ -3.14 & 1.35 & 8.86\\ -5.09 & 8.86 & 13.56\end{pmatrix}$	$\begin{pmatrix}-3.91 & -14.90 & 16.60\\ -14.90 & -0.52 & -12.03\\ 16.60 & -12.03 & 4.43\end{pmatrix}$

must increase according to the Lyddane-Sachs-Teller relation (and the known values of ϵ_0) when T drops below T_c.

In $LiNbO_3$ the *frozen-in* pattern of the ions below T_c shows that Li and Nb have moved along $+z$ and all O's have moved along $-z$. In Table V we give these displacements in Å using the data of Abrahams *et al.*[8] but have chosen a reference point such that the displacements conform to an optic mode (i.e., the center of mass does not shift). Above T_c then, in analogy with $SrTiO_3$, we would expect the strongest low-frequency mode to have these same displacements. The A_{2u} symmetry of this mode does not restrict the oxygen ions to move along the z axis, thus we must consider possible x, y motion for these ions as well as their z component of motion. From the x-ray work and symmetry considerations of Abrahams *et al.*, we conclude that above T_c the oxygen triangles we show in Fig. 7 are both the same size, while below T_c the upper triangle is larger than the lower one. We will assume then that the soft ferroelectric mode is as shown by the arrows in Fig. 7. The oxygen ions in the upper triangle move down and out while those in the lower triangle move down and in. For lack of more specific information we take the motion of the oxygen ions to be at 45° to the z axis, i.e., equal components of motion in the z direction and in the x-y plane. In Table V we list this motion though we emphasize that the ion displacements shown are only our estimation of the true normal mode. In the charge column we show the formal valency charge for $LiNbO_3$ (in contrast to an exact ion effective charge determined by a shell model fit as in $SrTiO_3$). We can now examine the Lorentz coefficients.[37] From Fig. 7 we note that the main bonds being compressed (as opposed to those undergoing bending motion) are the Li_1-O_4, O_5, O_6 bonds. In Table V we show the Lorentz local-field tensor $\beta(Li_1, O_6)$. Taking O_6 to move in the direction (using Cartesian coordinates) $x, y, z = (0, -1, -1)$ we find the local field (E_x, E_y, E_z) at the Li_1 side by adding the effect due to the y and z displacement,

$$(E_x, E_y, E_z) = (-3.14, 1.35, 8.86) + (-5.09, 8.86, 13.56) = (-8.23, 10.21, 22.42).$$

The x, y components of the local field at the Li_1 site do not contribute to the mode we are discussing and are canceled by the x, y fields at Li_1 due to O_4 and O_5. Each of O_4, O_5, O_6, however, does contribute a z-directed field of 22.42 (per unit polarization) which forces the Li_1^+ ion in the direction of its motion—i.e., lowers its restoring force. This is the most important Lorentz field in $LiNbO_3$, and the one we believe to be mainly responsible for the ferroelectric transition. There are other large Lorentz factors in the problem, for example $\beta(Li_1, O_1)$ has some large components. For the mode we are considering O_1, O_2, O_3 produce a field along $-z$ at Li_1, i.e., they raise the restoring force. However,

[37] Schweinler considered this problem earlier; however, he took $LiNbO_3$ to have the Ilmenite structure which leads to incorrect results. H. C. Schweinler, Phys. Rev. **87**, 5 (1952).

when we draw many primitive cells of the type shown in Fig. 7 stacked together, we find that Li_1 and O_1 occur as nearest neighbors in the same z plane. Thus, the mode involves a considerable bond bending motion for this ion pair. Thus, in analogy with $SrTiO_3$ we might expect that a large positive Lorentz factor is not needed here to favor instability.

Below T_c we would expect the softest mode to have again displacements somewhat like those shown in Fig, 7. The Lorentz factor $\beta(Li_1, O_6)$ still lowers the restoring. force arising from the Li_1-O_6 bond. We have evaluated the lattice sums for the Lorentz factors using the ion positions given in Fig. 7. Below T_c the zz component of $\beta(Li_1, O_6)$ is still positive but has decreased from 13.56 to 11.51. Similar to the case of $BaTiO_3$, however, some of the other bonds take on more stretching and less bending character because of the new ion positions. This effect tends to raise the mode frequency and the unusually large shifts which occur in the $LiNbO_3$ structure could account for the rather high frequency (248 cm^{-1}) for the A_1 mode at room temperature.

The displacements we have listed in Table V can be used to predict the spontaneous polarization P_s of the ferroelectric phase. From the displacement and charges in Table V, we calculate $P_s = 50\ \mu C/cm^2$ which is fairly large compared with other ferroelectrics but in line with the value P_s of the order of 300 $\mu C/cm^2$ recently deduced from a combination of pyroelectric and nonlinear optic measurements.[38]

V. CONCLUSIONS

The optical and Raman properties of $LiNbO_3$ have been investigated in the region 70 to 10 000 cm^{-1} and the results compared with group theoretical predictions. All expected infrared and Raman phonon modes are located except two. The index of refraction and the transparency region in the visible and near infrared have been shown to depend on the infrared phonons. The study of the phonon instabilities and Lorentz factors has suggested that the ferroelectric transition in $LiNbO_3$ is much like the transitions which occur in ferroelectric perovskites. In the perovskites above T_c, a certain phonon with polarization along [100], [010] or [001] has a large Lorentz factor which can lead to instability. In $LiNbO_3$, because of the distorted perovskite nature of the unit cell, it is a phonon very similar to the sum of these three perovskite phonons which has the large Lorentz factor which aids instability.

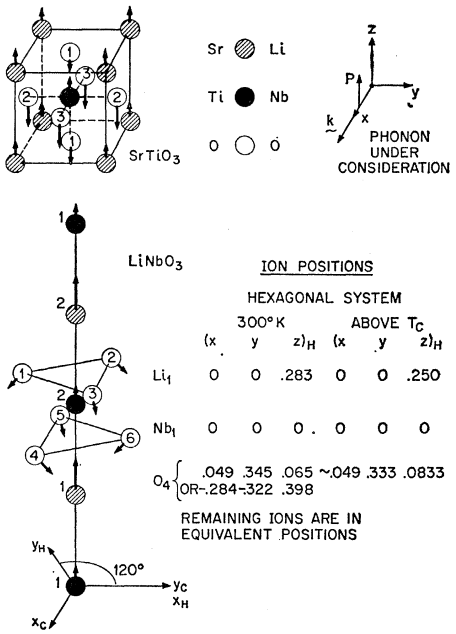

FIG. 7. Ion positions and unstable phonon-mode eigenvectors in $LiNbO_3$ and $SrTiO_3$. The primitive cell of each material is shown. For $SrTiO_3$ the eigenvector of Cowley's shell model is shown for the lowest-frequency (unstable) mode. In $LiNbO_3$ the lowest-mode eigenvector shown here represents the mode which goes unstable at T_c and is described in the text.

ACKNOWLEDGMENTS

The authors are grateful to K. Nassau, who kindly supplied the crystals used for these experiments. Helpful discussions were held with K. Nassau, S. C. Abrahams, and G. D. Boyd. We wish to thank R. E. Cox for performing the least-squares computer fits.

[38] R. C. Miller and A. Savage, *Proceedings of the International Meeting on Ferroelectricity* (Institute of Physics, Czechoslovak Academy of Sciences, Prague 1966).